Asian Journal of Current Research in Clinical Cancer
ISSN: 3062-4444
2023, Volume 3, Issue 1, Page No: 187-205
Copyright CC BY-NC-SA 4.0
Available online at: www.galaxypub.co/page/journals

Galaxy Publication

Galaxy Publication

Cellular Prion Protein (PrPC) Drives Epithelial–Mesenchymal Transition and EGFR-TKI Resistance in EGFR-Mutated Non-Small Cell Lung Cancer

Kenji Pereira[1]*, Wei P. Bianchi[1], Diego Garcia[1], Carlos H. Martinez[1], Lucia B. Li[1], Sofia X. Nakamura[1]

[1]Department of Hematology and Oncology, Faculty of Health and Medical Sciences, Charité – Universitätsmedizin Berlin, Berlin, Germany.

***E-mail** ✉ kpereira@hotmail.com

Received: 09 September 2023; **Revised:** 04 December 2023; **Accepted:** 09 December 2023

ABSTRACT

Patients diagnosed with EGFR-mutated non-small cell lung cancer (NSCLC) experience therapeutic advantages from EGFR-targeted tyrosine kinase inhibitors (TKIs). Even though third-generation agents like osimertinib have enhanced clinical outcomes, every patient eventually encounters tumor progression. Of the diverse pathways leading to TKI resistance, the role of epithelial-to-mesenchymal transition (EMT) is still not comprehensively defined. We postulated that the cellular prion protein, denoted PrPC, may contribute to EMT and resistance against EGFR-TKIs in NSCLC. Analyzing 5 separate lung adenocarcinoma datasets—one of which is our own collection—we confirm a correlation between PRNP gene expression (which codes for PrPC) and EMT signatures. Through alteration of PrPC amounts in multiple EGFR-mutated NSCLC cell models, we robustly demonstrate that PrPC is required for sustaining or developing mesenchymal characteristics. On a mechanistic basis, PrPC exerts its effects via an ILK-RBPJ pathway that simultaneously modulates EGFR levels. Additionally, our findings reveal higher PrPC abundance in EGFR-mutated tumors relative to wild-type counterparts, as well as increased expression upon EGFR stimulation in cell culture. We further establish that PRNP transcription escalates alongside acquired TKI resistance, while downregulation of PRNP renders cells more responsive to osimertinib. Moreover, in 2 distinct patient cohorts with EGFR-mutated NSCLC, circulating plasma PrPC concentrations were found to be elevated, and their changes over time paralleled disease trajectory. Taken together, these observations identify PrPC as a plausible facilitator of EMT-associated resistance to EGFR-TKIs in NSCLC. The results also imply that serial measurement of plasma PrPC could offer a practical, minimally invasive method for monitoring patients and justify evaluating therapies aimed at PrPC in EGFR-mutated NSCLC cases refractory to TKIs.

Keywords: Cellular Prion Protein (PrPC), Lung cancer, Epithelial–mesenchymal, EGFR-TKI

How to Cite This Article: Pereira K, Bianchi WP, Garcia D, Martinez CH, Li LB, Nakamura SX. Cellular Prion Protein (PrPC) Drives Epithelial–Mesenchymal Transition and EGFR-TKI Resistance in EGFR-Mutated Non-Small Cell Lung Cancer. Asian J Curr Res Clin Cancer. 2023;3(1):187-205. https://doi.org/10.51847/27lSdBu1hx

Introduction

Lung cancer persists as the primary cause of cancer mortality worldwide, responsible for 1.8 million fatalities in 2020 and accounting for 18% of total cancer deaths [1]. Given that most diagnoses occur at advanced stages involving inoperable or disseminated disease, the 5-year survival for non-small cell lung cancer (NSCLC)—the predominant form—hovers above 25% overall but plummets under 5% in stage 4 cases (https://seer.cancer.gov/statfacts/html/lungb.html). Enhanced molecular insights into NSCLC have uncovered actionable genetic changes, with EGFR mutations representing the most prevalent, affecting 15–25% of Caucasian patients and reaching 40 to 55% in East Asian populations [2]. Although mutant EGFR-directed TKIs, culminating in the third-generation drug osimertinib, have transformed management, acquired resistance develops universally in EGFR-mutant carriers, generally within 9–12 months [3, 4]. Established resistance pathways involve additional mutations, engagement of parallel signaling routes, epigenetic reprogramming, or phenotypic shifts [3, 4].

© 2023 Asian Journal of Current Research in Clinical Cancer

Phenotypic shifts prominently include epithelial-to-mesenchymal transition (EMT), originally noted in repeat biopsies from progressing EGFR-driven NSCLC [5, 6], substantiated experimentally in culture systems [7], and lately recognized as characteristic of persister cell populations in single-cell profiling [8]. In line with this, numerous laboratory-based reports indicate that induction of EMT promotes evasion of EGFR-TKI effects (as summarized in [9, 10]), whereas interventions that block EMT can re-establish vulnerability to EGFR blockade in NSCLC models [7, 11-13]. Still, the precise regulators and mediators governing EMT in this setting are incompletely mapped [14].

Recently, the cellular prion protein PrPC has gained attention for facilitating EMT in several malignancies [15]. Notably, our prior work revealed selective PRNP upregulation in mesenchymal colorectal tumors and its governance over the core EMT regulator ZEB1 [16]. Multiple investigations have also underscored PrPC's capacity to foster migration and invasion in tumor cells [15] (for review). Within lung cancer contexts, Lin and colleagues reported greater PrPC abundance in aggressive cell lines versus indolent ones, along with its stimulation of lamellipodia [17]. Nonetheless, the connections linking PrPC to EMT in lung malignancies, and its wider implications for lung cancer traits, require further clarification.

The present investigation aimed to delineate PrPC functions in lung adenocarcinoma (LUAD). We undertook broad-scale evaluations to detect gene expression and protein patterns tied to PRNP levels and EMT in LUAD. Cellular experiments were deployed to probe PRNP's influence on EMT dynamics and its crosstalk with EGFR signaling. Lastly, bioinformatics approaches, laboratory testing, and quantification of soluble PrPC in patient plasma were merged to gauge PrPC's involvement in TKI refractoriness among EGFR-mutated LUAD cases. In summary, this study characterizes PrPC as an inducer of mesenchymal shifting and linked EGFR-TKI escape. It raises the possibility that PRNP itself, or activated cascades downstream of it, might function as diagnostic indicators or intervention points to circumvent resistance in LUAD.

Materials and Methods

Reagents

The compound QLT0267 was generously provided by Dr. Shoukat Dedhar. The working concentration of QLT0267 was selected based on earlier titration experiments [18]. Recombinant human TGFβ1 was acquired from R&D Systems (Minneapolis, MN, USA) (cat. no. 240-B) and solubilized as per the vendor's protocol in 4 mM HCl supplemented with 1 mg/ml BSA. HCC827 cultures received 10 ng/ml TGFβ or matching vehicle (HCl/BSA) for 24 h. Recombinant human EGF was obtained from R&D Systems (cat. no. 236-EG-200) and prepared in PBS according to instructions. H1650 cultures were challenged with 25 ng/ml EGF or PBS vehicle for 24 h.

Osimertinib (AZD-9291/mereletinib, 5 mg) was bought from MedChemExpress (Princeton, NJ, USA) and stocked in DMSO.

Cell culture

Non-small cell lung carcinoma lines H1650, HCC827, and H1975 were sourced from the American Type Culture Collection and propagated in RPMI-1640 medium. The colorectal line MDST8 and prostate line PC3 were obtained from Sigma; MDST8 was maintained in DMEM while PC3 used RPMI-1640. Every medium contained 10% (v/v) FBS (Gibco, France) plus 1% (v/v) penicillin-streptomycin (Gibco, France). Cultures were kept at 37 °C under 5% CO_2 in humidified conditions and periodically checked for mycoplasma absence. Oncogenic driver mutations were verified via NGS employing a targeted AmpliSeq panel (WG_IAD196383V2; 119 amplicons spanning 23 cancer-related genes; Life Technologies-Thermo Fisher Scientific). For short-term gene knockdown, cells received 50 nM siRNA delivered with Lipofectamine 2000 (Invitrogen) per vendor guidelines. Employed sequences included 5′-CAGUACAGCAACCAGAACA-3′ (siPRNP sense) and 5′-AACGAUGACACGAACACAC-3′ (scrambled sense control). Samples for RNA or protein analysis were taken 72 h after transfection. Silencer Select siRNA targeting JAG1 (Assay ID 146914) was purchased from Thermo Fisher Scientific.

Preparation of protein extracts and western blot analyses

After PBS washing, cells were extracted on ice for 30 min in NaDOC buffer [50 mM Tris·HCl (pH 7.4), 150 mM NaCl, 5 mM EDTA, 0.5% Triton X-100, 0.5% sodium deoxycholate] containing phosphatase inhibitors (Thermo

Fisher Scientific, Waltham, MA, USA) and protease inhibitors (Roche, Mannheim, Germany). Debris was removed by spinning at 14,000 × g for 15 min. Supernatant protein was quantitated via bicinchoninic acid assay (Pierce, Rockford, IL, USA). Samples (15 µg protein) were fractionated on 4–12% gradient SDS-PAGE gels (Invitrogen), then blotted onto nitrocellulose using the iBlot system (Invitrogen). Non-specific sites were blocked for 1 h at ambient temperature with SEA BLOCK reagent (Thermo Fisher Scientific), followed by primary antibody probing for 1 h at ambient temperature. Signals were developed with IRDye-labeled secondary antibodies (Li-Cor Biosciences, Lincoln, NE, USA) and captured on an Odyssey scanner (Li-Cor Biosciences).

Isolation of total RNA and RT-PCR analysis

Total RNA was purified with the RNeasy kit (Qiagen, Limburg, Netherlands) following the provided procedure. cDNA synthesis employed oligo(dT)/random hexamer priming with the SensiFAST kit (Meridian, Memphis, TN, USA). Quantitative PCR reactions used ABsolute QPCR SYBR Green ROX master mix (Thermo Scientific, Waltham, MA, USA) run on a QuantStudio 12 K Flex platform (Applied Biosystems, Life Technologies Corporation, Carlsbad, CA, USA). Cycle data were processed with SDS 2.3 software (Applied Biosystems). Target expression was normalized to RPL13A and computed by the ΔΔCt approach.

Immunofluorescence and confocal microscopy

H1975 cells seeded on coverslips were fixed using 4% paraformaldehyde in PBS, then blocked in PBS with 1% BSA and 20 mM glycine. Permeabilization involved 0.1% Triton X-100 in PBS/glycine for 15 min. Anti-PrPC antibody (12F10, Bertin Pharma, Montigny Le Bretonneux, France) was diluted 1/20 and anti-EGFR (#4267, Cell Signaling, Danvers, MA, USA) 1/50 in PBS containing 1% BSA and 0.1% Tween, applied for 1 h. Detection used Alexa Fluor 488/555 secondaries co-incubated for 1 h with TRITC-phalloidin to visualize actin. DNA was labeled with DAPI. Standard fluorescence was imaged on a Zeiss Axio Observer Z1 microscope; confocal stacks were acquired on a Zeiss LSM 710. All images were adjusted using FIJI.

Cell sensitivity to osimertinib

H1975 cells were seeded for 24 h, switched to low-serum medium (1% FBS) for 24 h, then transfected with siRNA. One day later, graded osimertinib doses or DMSO control were added for 72 h. Viable cell parameters (count, size, volume) were measured with a CASY TT counter (Schärfe System GmbH, Reutlingen, Germany).

Real-time cell migration and invasion

Dynamic migration/invasion monitoring employed CIM-Plate 16 wells on an xCELLigence RTCA DP analyzer (Agilent, Santa Clara, CA, USA) as directed by the supplier. Upper chambers received 20,000 H1975 cells in medium with 3% FBS; lower chambers contained 10% FBS as chemoattractant. Invasion setups included a 30 µl layer of diluted Cultrex (1:15 in medium; Biotechne, Minneapolis, MN, USA) on the upper membrane. Electrical impedance was logged every 15 min across 48 h. Each condition was tested in triplicate.

3′ RNA sequencing

Polyadenylated RNA sequencing libraries were constructed employing the Lexogen Quant-Seq 3′ mRNA-Seq Library Prep Kit FWD for Illumina, in compliance with the protocol provided by the manufacturer. The prepared libraries underwent sequencing on the NovaSeq6000 platform. The resulting FASTQ files from RNA sequencing were processed via a conventional bioinformatics workflow, incorporating adjustments tailored to polyA-selected data. In summary, alignment of reads was achieved with STAR software (version 2.7.9a) [19]. Genes lacking an official HGNC symbol were excluded from further consideration. Downstream analyses were executed utilizing the DESeq2 package (version 1.38.3) within R Studio version 4.2.2.

Gene expression analyses

Datasets limited exclusively to lung adenocarcinoma (LUAD) samples from cell lines and patients were sourced from publicly available repositories: the Cancer Cell Line Encyclopedia (CCLE) (n = 45) [20], The Cancer Genome Atlas (TCGA) (n = 511) [21], the Onco-HEGP cohort (n = 107) [22], as well as patient samples from the proteogenomic investigations conducted by Chen *et al*. (n = 90) [20] and Lehtiö *et al*. (n = 90) [23]. Supplementary datasets comprised GSE49644 [24], GSE121634 [13], GSE131594 [25], GSE193258 [26], GSE17373 [27], and

PRJNA591860 [28]. Gene Set Enrichment Analysis (GSEA) was executed via the platform hosted by the Broad Institute (http://www.broadinstitute.org/gsea/index.jsp; Version 2.0.14).

Collection of blood samples and analysis of plasma PrPC

The study involved plasma specimens obtained from 29 individuals diagnosed with EGFR-mutated metastatic non-small cell lung cancer (NSCLC) who underwent first-line treatment with EGFR tyrosine kinase inhibitors (EGFR-TKI). Every procedure adhered to applicable guidelines and regulatory standards. Of these, 17 patients were part of the "PLAPOU" cohort, whereas the remaining 12 originated from the Onco-HEGP collection. Enrollment for the PLAPOU cohort occurred prospectively from June 2013 to November 2015 at Hôpital Européen Georges Pompidou (HEGP), with prior documentation available [29]. Approval for blood collection was granted by the Ile-de-France II Ethics Committee for the Protection of Persons (CPP Ile-de-France II n°2013-06-21 SC), and all participants provided written informed consent. The additional patient subset was derived retrospectively from stored clinical plasmas at Onco-HEGP. Patient consent was documented, and the collection was authorized by the Ile-de-France II Ethics Committee (CPP Ile-de-France II n°2013-A01283-42), including acquisition of written informed consent. Specimens were furnished by the Biological Resources Center and Tumor Bank Platform (BB-0033-00063). For controls, plasma from 71 healthy volunteers of comparable age and without signs of malignancy was included [16]. Plasma aliquots were maintained at −70 °C prior to testing. Quantification of PrPC in plasma was accomplished using the DELFIA assay, following the methodology outlined in [16]. All assays were performed in a blinded manner. Circulating tumor DNA (ctDNA) evaluation in the Onco-HEGP cohort patients followed the approach described in [29].

Statistical analyses

Computational statistical evaluations were carried out in R Studio (version 4.2.2) by means of the stat_compare_means function within the ggpubr package. Data derived from cell line experiments are displayed as mean values ± standard error of the mean (s.e.m.), with visualizations produced in GraphPad PRISM (version 9.4.1). Pairwise group comparisons involved initial assessment of normality via the Shapiro-Wilk test, succeeded by either Student's t-test or the Mann-Whitney rank-sum test depending on the distribution. Findings from public databases or clinical cohorts are depicted as medians accompanied by interquartile ranges, with figures generated using ggplot2 in R Studio. Hypothesis testing utilized the Mann-Whitney rank-sum test for comparisons between two groups, or one-way ANOVA supplemented by pairwise Wilcoxon rank-sum tests adjusted via Holm's method when analyzing more than two groups.

Results and Discussion

Cellular prion protein (PrP^C) is linked to epithelial-mesenchymal transition (EMT) in non-small cell lung cancer (NSCLC)

To determine if PRNP expression relates to EMT, we applied Gene Set Enrichment Analysis (GSEA) to multiple lung adenocarcinoma (LUAD) datasets from both cell lines and patients. The analyzed collections included 45 LUAD cell lines from the Cancer Cell Line Encyclopedia (CCLE) [20], 511 LUAD cases from The Cancer Genome Atlas (TCGA), 107 LUAD samples from the Onco-HEGP cohort [22], 90 tumors from the proteogenomic analysis conducted by Chen *et al*. [30], and another 90 LUAD tumors from the proteogenomic work by Lehtiö *et al*. [23]. Strikingly, elevated PRNP mRNA showed a robust and reproducible connection to EMT signatures in every dataset examined **(Figures 1a and 1b)**. Supporting this, PRNP transcript abundance displayed strong positive relationships with major EMT-regulating transcription factors, especially SNAI2, ZEB1, and ZEB2, throughout the collections **(Figure 1c)**. At the protein level, similar robust associations emerged between PrP^C and SLUG (product of SNAI2), ZEB1, or ZEB2 based on data from Chen *et al*. [30] and Lehtiö *et al*. [23]. Across all clinical series, PRNP levels inversely related to the epithelial EMT score (EMT_epi) while directly relating to the mesenchymal EMT score (EMT_mes), consequently aligning with the broader pan-cancer EMT signature (EMT_score) introduced by Mak *et al*. [31] **(Figure 1d)** and with an alternative mesenchymal metric (mes_score) reported by de Reyniès *et al*. [32] **(Figure 1d)**. Within the Onco-HEGP series, tumors classified as mixed or mesenchymal exhibited markedly higher PRNP mRNA than those deemed epithelial. Additionally, PRNP expression rose in samples showing weak miR-200 activity versus strong activity, where

reduced miR-200 correlates with worse survival [24]. Collectively, these computational findings strongly indicate that PRNP activity ties closely to EMT processes in LUAD.

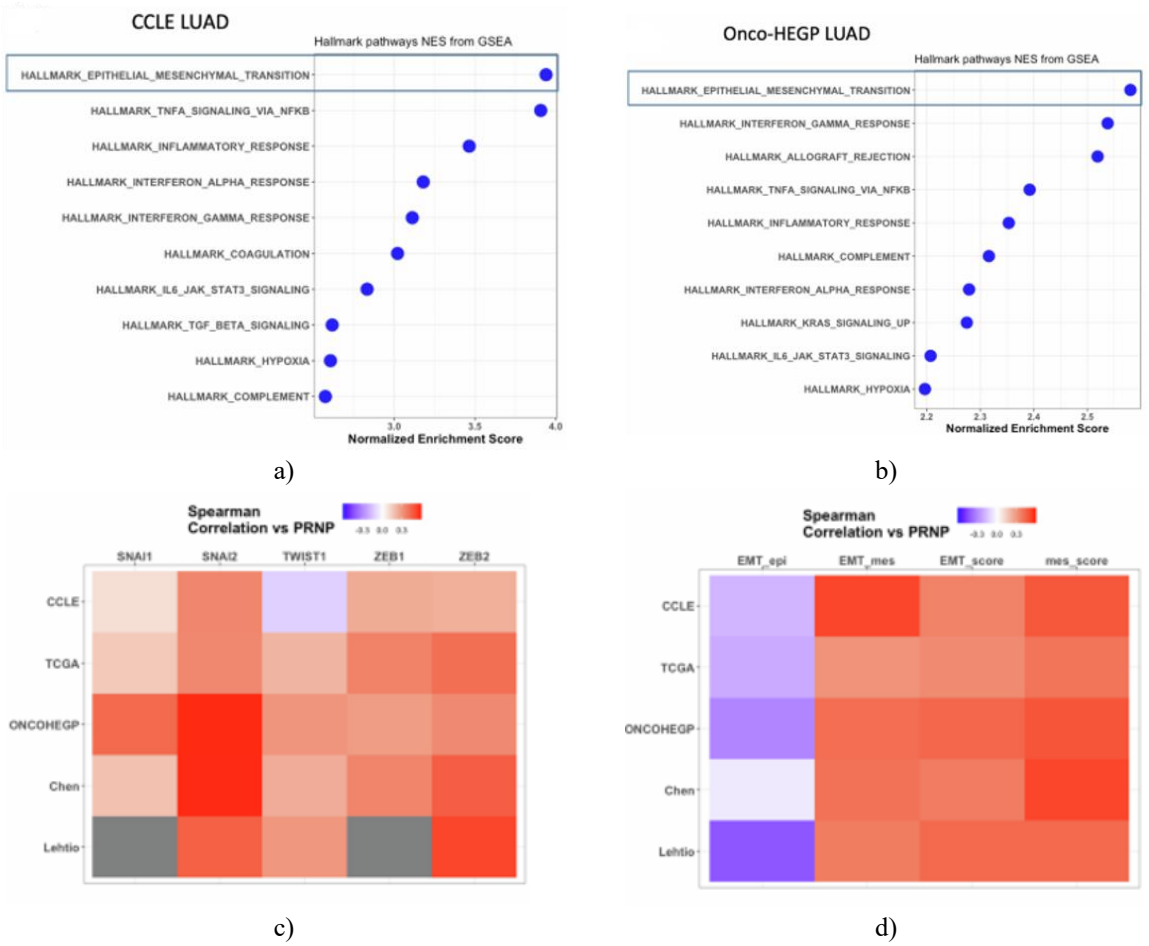

Figure 1. Association between PRNP expression and EMT features in LUAD.
GSEA results illustrating EMT signature enrichment among genes co-varying with PRNP in CCLE-derived LUAD lines (a) and Onco-HEGP patient samples (b). c) Summary heatmap of correlation values linking PRNP to various EMT transcription factors across datasets. d) Summary heatmap of correlation values connecting PRNP to pan-cancer epithelial (EMT-epi), mesenchymal (EMT-mes), overall EMT scores per Mak *et al*. [31], and the mesenchymal metric per de Reyniès *et al*. [32] across datasets.

PrP^C depletion suppresses EMT in NSCLC models

To explore whether PrP^C plays an active role in driving EMT, we turned to in vitro experiments. We focused on LUAD lines harboring EGFR mutations to also probe potential ties to EGFR-TKI resistance. The selected models—H1975, HCC827, and H1650—carry specific EGFR changes. The H1975 line, characterized by abundant PrP^C and inherent mesenchymal traits, responded to PRNP-targeted siRNA with sharp downregulation of key EMT drivers including SNAI2, TWIST1, ZEB1, and ZEB2 at the mRNA level **(Figure 2a).** This was validated protein-wise for ZEB1 **(Figure 2b)** and SLUG (SNAI2 product) **(Figure 2c).** Global gene expression profiling combined with GSEA revealed that removing PrP^C notably weakened the overall EMT program in these cells **(Figure 2d).** Visually, depleted cells adopted a broader, more spread-out appearance relative to controls **(Figure 2e).** Quantitative assessment via CASY TT showed fewer cells upon PRNP knockdown **(Figure 2f)** alongside larger individual cell volumes **(Figure 2g),** matching the shape shift noted earlier. Real-time tracking of motility and invasiveness with xCELLigence revealed profound deficits in both properties after siPRNP treatment **(Figures 2h and 2i).**

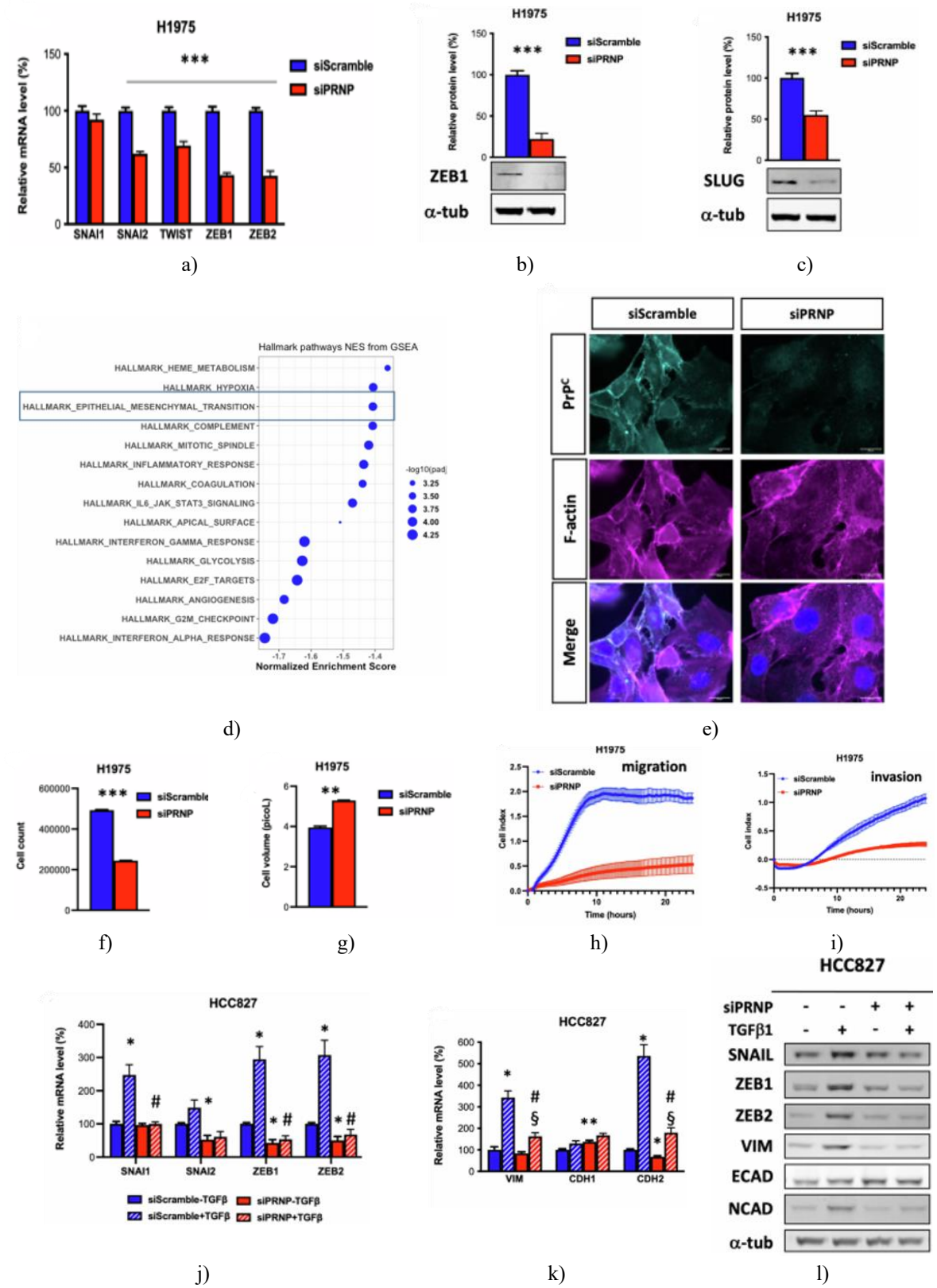

a) b) c)

d) e)

f) g) h) i)

j) k) l)

Figure 2. PrP^C supports maintenance of EMT in LUAD lines.

a) Quantitative RT-PCR measuring EMT transcription factors SNAI1, SNAI2, TWIST, ZEB1, and ZEB2 in H1975 cells after PRNP knockdown versus controls. Protein detection via Western blot for ZEB1 (b) and SLUG (c) under the same conditions. d) GSEA pinpointing EMT pathways as highly disrupted following PRNP loss in H1975. e) Fluorescence microscopy of PrP^C and F-actin distribution in knockdown versus control H1975. CASY-based quantification indicating lower cell counts (f) but greater volume (g) post-knockdown. Real-time cell index tracking during migration (h) and invasion (i) assays in xCELLigence for

knockdown versus control H1975. Further qRT-PCR evaluating EMT regulators SNAI1, SNAI2, ZEB1, ZEB2 (j) plus marker genes VIM, CDH1, CDH2 (k) in HCC827 under combined PRNP siRNA and TGFβ1 stimulation. L Corresponding Western blots for SNAIL, ZEB1, ZEB2, Vimentin, E-cadherin, and N-cadherin in HCC827 with the same treatments. Data shown as means ± s.e.m from n = 2 independent triplicates (a–c, J) or n = 1 triplicate (F–I, L). *p < 0.05, **p < 0.01 ***p < 0.001 vs. control (siScramble), #p < 0.05, ###p < 0.001 vs. TGFβ1-treated siScramble, §p < 0.05 vs. untreated knockdown. Western signals normalized to α-tubulin (α-tub)

After establishing that PrP^C in the inherently mesenchymal H1975 cells is critical for preserving mesenchymal traits, we proceeded to test if PrP^C is also needed for inducing such traits upon exposure to cytokines. We chose the HCC827 model, widely recognized for TGFβ-triggered EMT. Examination of publicly available data from Sun *et al*. (GSE49644) [33] showed marked elevation of PRNP alongside major EMT regulators in HCC827 cells that had fully shifted to mesenchymal status after extended TGFβ treatment. In our shorter protocol (10 ng/ml TGFβ for 24 h), HCC827 cells robustly increased SNAI1, ZEB1, ZEB2, VIM, and CDH2 expression **(Figures 2j and 2k).** Critically, knocking down PrP^C blocked TGFβ-mediated induction of these transcription factors entirely **(Figure 2j)** and strongly blunted VIM and CDH2 upregulation **(Figure 2k).** Moreover, PrP^C-deficient cells retained elevated CDH1 transcript and E-cadherin protein **(Figures 2k and 2l).** Immunoblotting verified that TGFβ-driven protein increases in SNAIL, ZEB1, ZEB2, Vimentin, and N-cadherin were eliminated by PrP^C depletion **(Figure 2l)**. Matching immunofluorescence for Vimentin, E-cadherin, and N-cadherin in TGFβ-challenged HCC827 cells with or without PrP^C loss reinforced these outcomes.

Of interest, acute TGFβ administration left PrP^C transcript and protein unchanged, implying that the PRNP rise reported by Sun *et al*. occurs downstream as a secondary event. This further indicates that boosted PrP^C is not obligatory for initial EMT engagement in this system; rather, the relatively low constitutive PrP^C—much less than in H1975 renders cells competent to mount an EMT response to TGFβ. RNA sequencing with GSEA on HCC827 cells ± PrP^C ± TGFβ confirmed equivalent TGFβ pathway engagement regardless of PrP^C status, arguing against direct interference with canonical TGFβ transduction. Instead, PrP^C likely modulates a parallel synergistic arm, as evidenced by persistent (though attenuated) TGFBI induction by TGFβ in knockdown cells—in stark contrast to the total absence of EMT regulator activation **(Figure 2j).** Together, these results affirm PrP^C as indispensable for either sustaining (H1975) or initiating (HCC827) mesenchymal programs in NSCLC, consistent with the bioinformatic associations in **Figure 1.**

PrP^C modulates NOTCH signalling in NSCLC via ILK

Our data reveal PrP^C as essential for EMT regulator activation under TGFβ influence in NSCLC and imply facilitation of crosstalk with an auxiliary pro-EMT route. Several clues directed us toward NOTCH involvement. We had earlier demonstrated PrP^C governance of NOTCH activity in vitro and in vivo [34], echoed by Wang *et al*. in pancreatic models [35]. NOTCH participation in EMT onset and persistence in NSCLC is well substantiated [10]. Cooperative interplay between NOTCH and TGFβ during EMT is recognised [36], and accordingly, depleting the ligand JAG1 diminished TGFβ-driven EMT in HCC827. RNAseq coupled with GSEA disclosed NOTCH pathway suppression after PRNP loss in H1975 **(Figure 3a).** In Onco-HEGP samples, non-epithelial (mixed/mesenchymal) tumors expressed significantly more JAG1, NOTCH2, and the mediator RBPJ [37] than epithelial ones, with each correlating positively to PRNP. Comparable trends, including strong protein-level links (>0.50) between PrP^C and NOTCH2/RBPJ in the Chen cohort, appeared across Chen and Lehtiö proteogenomics.

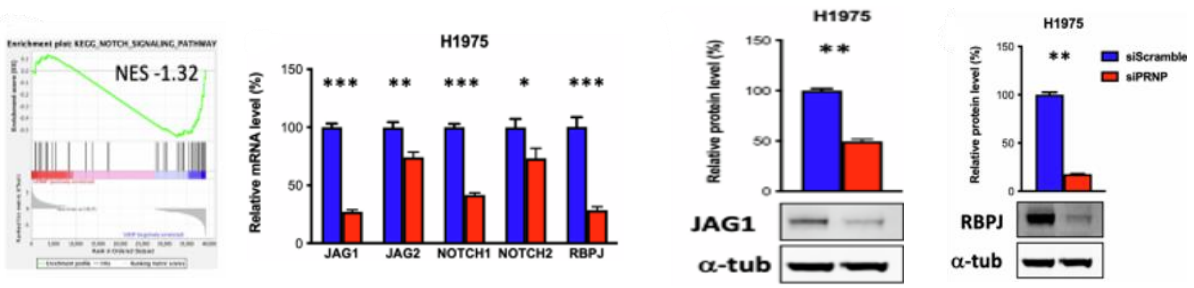

a) b) c) d)

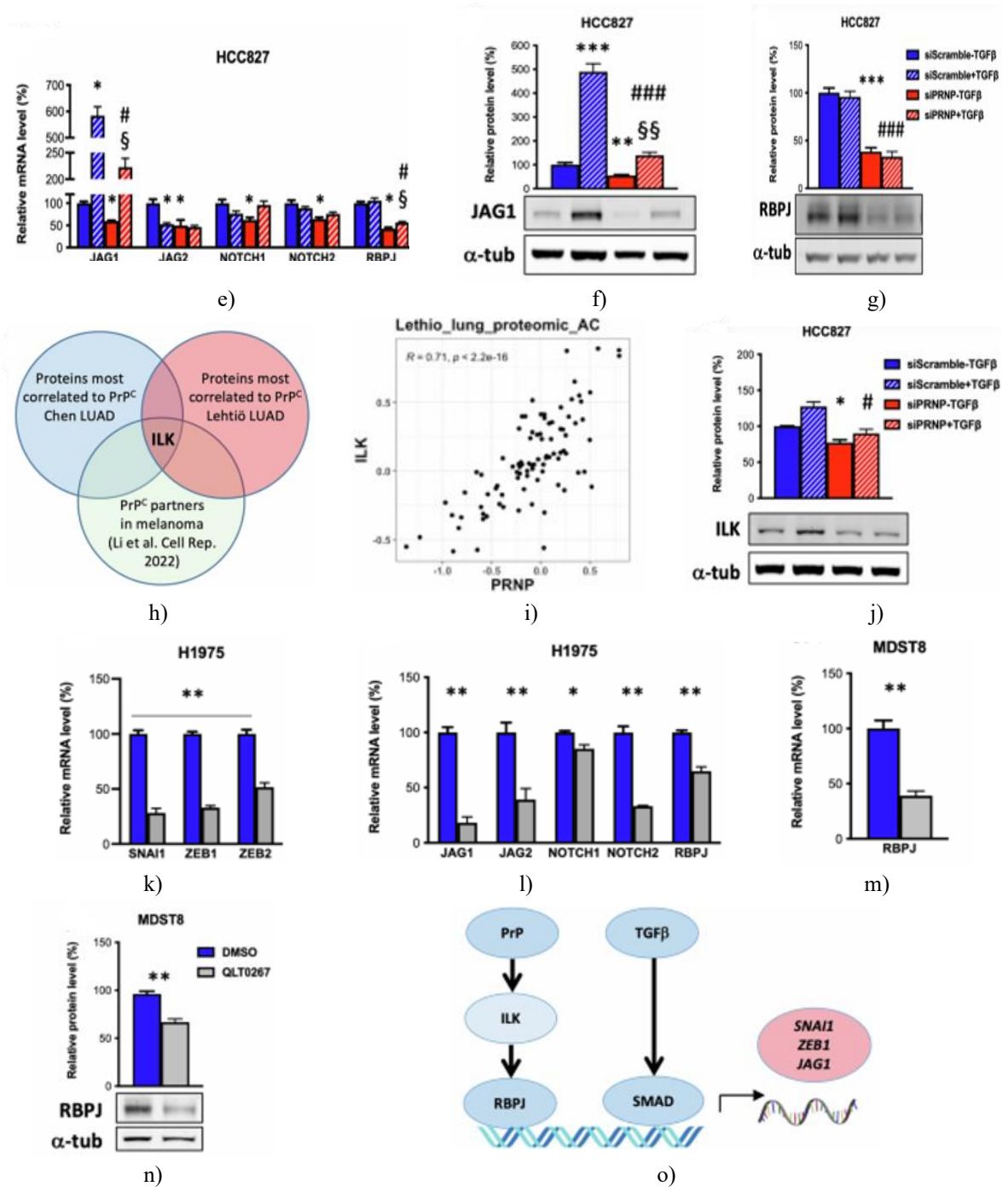

Figure 3. PrP^C directs EMT in LUAD models through an ILK-RBPJ route.

a) GSEA demonstrating NOTCH pathway perturbation upon PRNP depletion in H1975. B qRT-PCR quantifying JAG1, JAG2, NOTCH1, NOTCH2, and RBPJ in knockdown versus control H1975. Immunoblots for JAGGED1 (c) and RBPJ (d) in the same setting. qRT-PCR evaluating JAG1, JAG2, NOTCH1, NOTCH2, and RBPJ (e) with immunoblots for JAGGED1 (f) and RBPJ (g) in HCC827 under PRNP siRNA ± recombinant TGFβ1. H Venn overlap pinpointing ILK as the leading shared correlate of PrP^C abundance in Chen/Lehtiö proteomics and established PrP^C binder in melanoma. Correlation scatter for ILK versus PrP^C protein in Lehtiö data (i). Immunoblot detecting ILK in HCC827 with PRNP siRNA ± TGFβ1 (j). qRT-PCR measuring EMT regulators SNAI1, ZEB1, ZEB2 (k) and NOTCH components JAG1, JAG2, NOTCH1, NOTCH2, RBPJ (l) in QLT0267-exposed versus vehicle H1975. qRT-PCR (m) plus immunoblot (n) for RBPJ in QLT0267 versus control MDST8. o) Model outlining PrP^C orchestration of downstream EMT regulators. qRT-PCR and immunoblot results are means ± s.e.m from n = 2 independent triplicates. *p < 0.05, **p < 0.01, ***p < 0.001 vs.

control (siScramble or vehicle), #p < 0.05, ###p < 0.001 vs. TGFβ1-exposed siScramble, §p < 0.05, §§p < 0.01 vs. TGFβ1-naïve knockdown. Immunoblot quantification normalised to α-tubulin (α-tub).

To confirm these findings, we demonstrated that H1975 cells with PrP^C knockdown displayed markedly decreased mRNA abundance of NOTCH ligands JAG1 and JAG2, receptors NOTCH1 and NOTCH2, and downstream mediator RBPJ relative to control H1975 cells **(Figure 3b).** Protein reductions were verified for JAG1 **(Figure 3c)** and RBPJ **(Figure 3d).** This PrP^C-mediated regulation of NOTCH components in mesenchymal tumour cells appears widespread. Consistent patterns emerged in PC3 prostate carcinoma cells, where PrP^C depletion reversed mesenchymal traits and lowered multiple NOTCH effectors. In HCC827 cells, baseline JAG1 mRNA and protein dropped upon PrP^C loss **(Figures 3e and 3f).** As previously reported [38], TGFβ strongly elevated JAG1 transcript and protein **(Figures 3e and 3f),** but this induction was substantially weakened in PrP^C-depleted cells **(Figures 3e and 3f).** Sethi *et al*. [30] established that TGFβ-driven JAG1 upregulation involves canonical SMAD signalling. A complete PrP^C dependence on SMAD recruitment to the JAG1 promoter would predict total loss of responsiveness in knockdown cells, which did not occur. A more plausible scenario is that PrP^C activates a parallel cascade synergising with TGFβ for optimal JAG1 induction. Notably, RBPJ itself binds the JAG1 promoter [39]. Mirroring results in H1975 lung **(Figure 3d)** and PC3 prostate lines, RBPJ mRNA and protein declined sharply in PrP^C-silenced HCC827 cells under both resting and TGFβ-stimulated conditions **(Figures 3e and 3g).** Thus, PrP^C governance of RBPJ may drive subsequent JAG1 control. This prompted investigation into how PrP^C regulates RBPJ. Considering immediate PrP^C mediators, we focused on Integrin-Linked Kinase (ILK), given our prior evidence of ILK transmitting PrP^C signals in mesenchymal colorectal carcinoma [18] and its recent identification in PrP^C interactomes from two melanoma lines [40]. Strongly backing this idea, PrP^C and ILK proteins correlated tightly across two LUAD proteogenomic collections **(Figures 3h and 3i)**. ILK protein also fell in PrP^C-knockdown HCC827 cells and no longer rose with TGFβ **(Figure 3j).** Treating H1975 cells with the selective ILK blocker QLT0267 [41] tested ILK influence on EMT regulators and NOTCH elements. Inhibited cells showed clear drops in SNAI1, ZEB1, and ZEB2 transcripts **(Figure 3k)** plus broad suppression of NOTCH players, especially JAG1 **(Figure 3l).** In MDST8 colorectal carcinoma, where ILK serves as primary PrP^C effector [18], QLT0267 similarly lowered RBPJ mRNA and protein **(Figures 3m and 3n).** RBPJ reportedly binds the ZEB1 promoter directly [42], and its depletion reduces SNAIL and ZEB1 [43]. Collectively, these data support PrP^C engagement of an ILK-RBPJ module that synergises with TGFβ to orchestrate EMT transcription factors and JAG1 **(Figure 3o).**

Bidirectional crosstalk exists between PrP^C and EGFR pathways in NSCLC

Deeper inspection of GSEA outputs revealed consistent enrichment of an EGFR activation gene set (EGFR_UP.V1_UP) among transcripts co-varying with PRNP across CCLE lines and all clinical series **(Figure 4a)**. This could reflect EGFR-driven PrP^C upregulation, PrP^C enhancement of EGFR activity, or both. CCLE LUAD lines exhibited higher PRNP mRNA in EGFR-mutant versus wild-type counterparts **(Figure 4b),** a pattern repeated in Onco-HEGP patients **(Figure 4b).** Proteogenomic analyses by Chen *et al*. and Lehtiö *et al*. [23, 30] disclosed substantially elevated PrP^C protein in EGFR-mutant tumours compared to wild-type cases **(Figure 4c).** Mouse Prnp similarly rose in lungs bearing L858R, T790M, or compound EGFR-mutant tumours relative to normal tissue (GSE17373 dataset, [27]) **(Figure 4d).** NOTCH2 and ILK also increased significantly in EGFR-mutant samples in two of three cohorts.

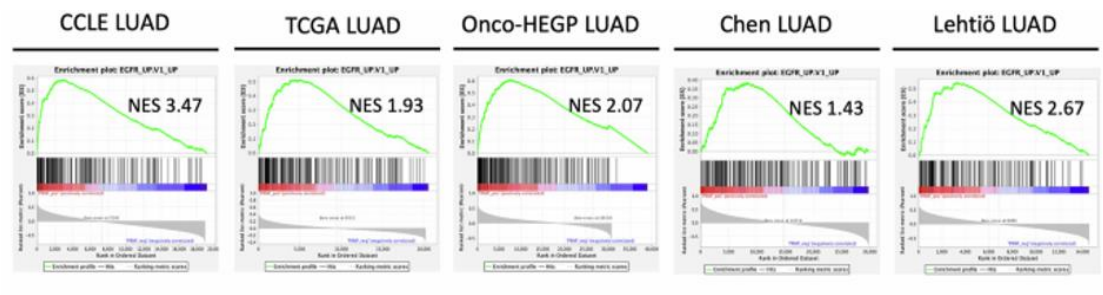

a)

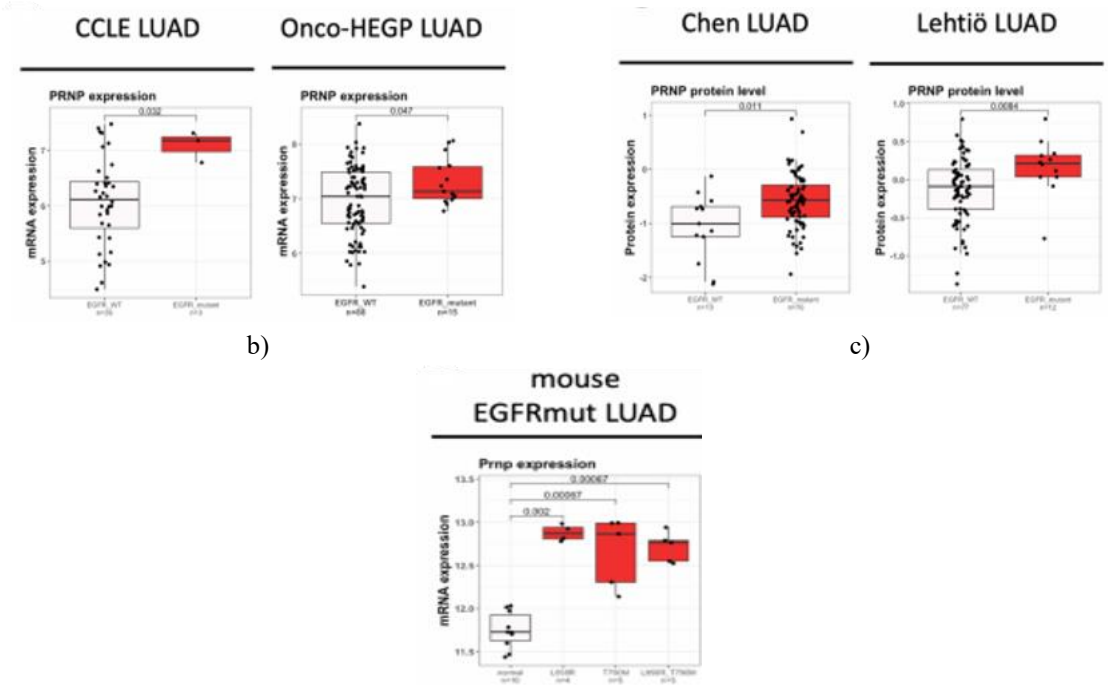

Figure 4. PRNP abundance aligns with EGFR activity and rises in EGFR-mutant LUAD. a) GSEA revealing EGFR activation signature (EGFR_up.V1_up) enrichment among PRNP-correlated genes in CCLE LUAD lines and TCGA, Onco-HEGP, Chen, or Lehtiö LUAD patient sets. b) Boxplots depicting PRNP transcript distribution by EGFR mutation status in CCLE and Onco-HEGP LUAD. c) Boxplots of PrP^C protein distribution by EGFR status in Chen and Lehtiö LUAD. d) Boxplot of mouse Prnp transcript in lungs from EGFR L858R, T790M, or double-mutant LUAD models.

Reinforcing potential EGFR induction of PrP^C, EGF stimulation (25 ng/ml, 24 h) of H1650 cells boosted PRNP mRNA and PrP^C protein **(Figures 5a and 5b);** this treatment also triggers EMT [44]. Conversely, testing PrP^C influence on EGFR across H1650, HCC827, H1975, and PC3 lines showed PRNP knockdown lowered EGFR transcripts **(Figures 5c)**. Protein decreases occurred in H1975 and PC3 **(Figure 5d)**, while HCC827 knockdown cells lost the ability to elevate EGFR mRNA/protein under TGFβ **(Figures 5e and 5f),** paralleling EMT regulators. ILK inhibition via QLT0267 in H1975 sharply cut EGFR mRNA **(Figure 5g).** We therefore propose PrP^C-ILK-RBPJ governance of EGFR **(Figure 5h),** consistent with prior NOTCH-mediated EGFR control by us [35] and others [45].

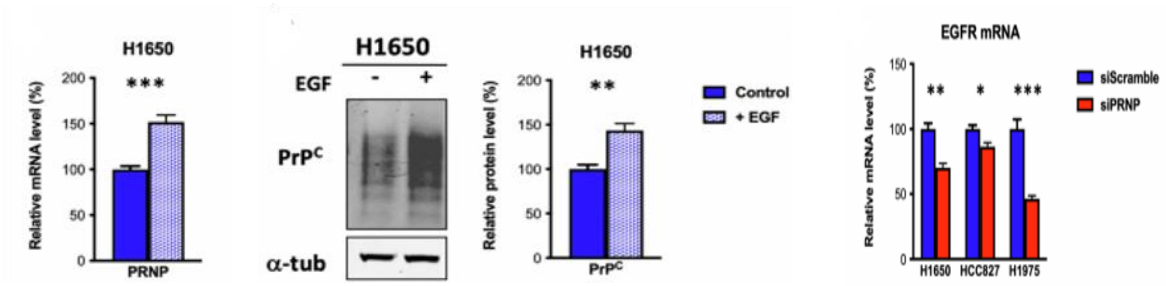

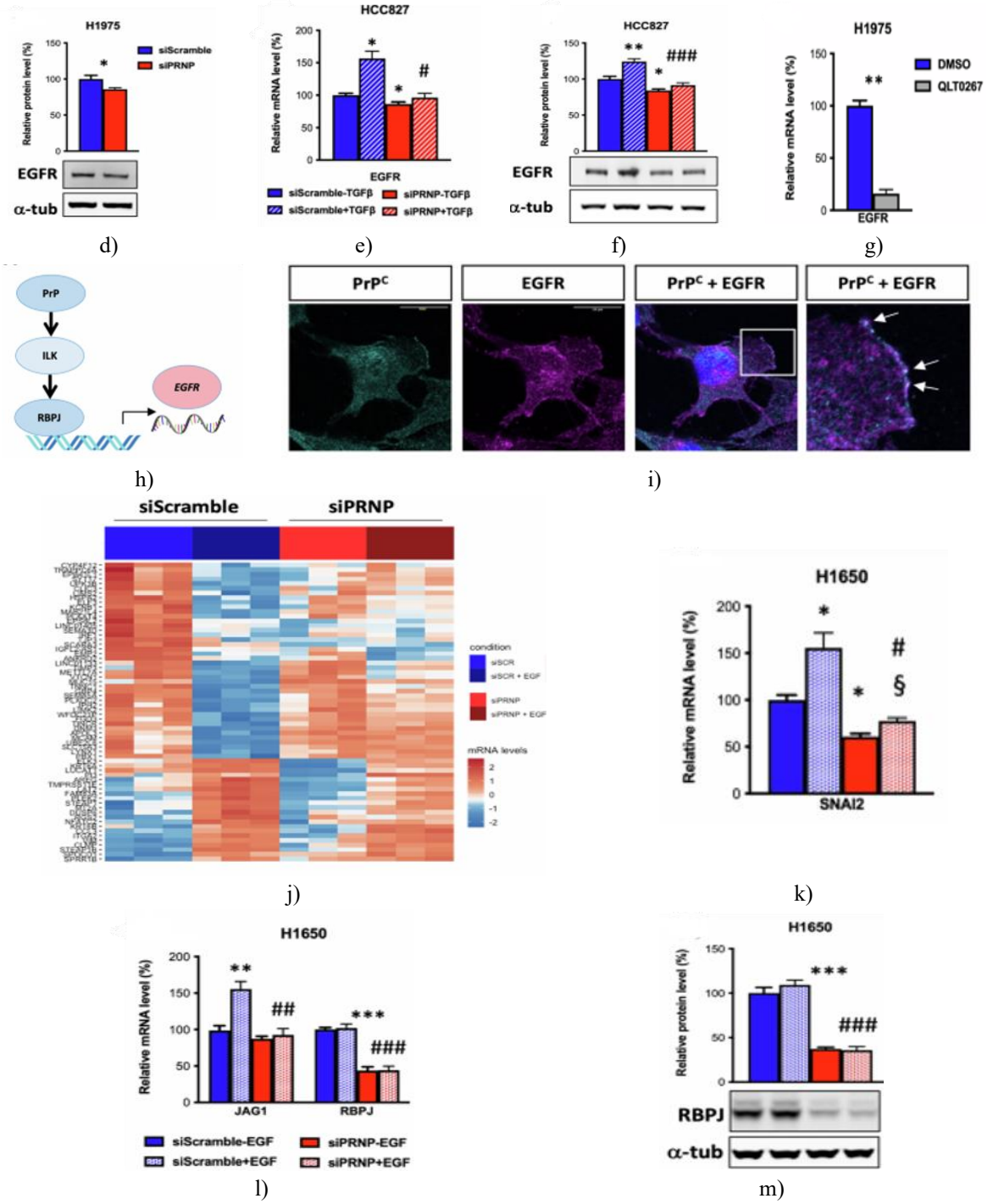

Figure 5. Mutual regulatory, physical, and functional ties link PrP^C and EGFR. qRT-PCR (a) and immunoblot (b) assessing PRNP/PrP^C in EGF-exposed versus untreated H1650. C qRT-PCR measuring EGFR transcript in PRNP-depleted H1650, HCC827, and H1975 versus controls. d) Immunoblot of EGFR protein in PRNP-knockdown H1975 versus control. qRT-PCR (e) and immunoblot (f) evaluating EGFR in HCC827 under PRNP siRNA ± recombinant TGFβ1. G qRT-PCR of EGFR transcript in QLT0267-exposed versus vehicle H1975. h) Model proposing EGFR control via PrP^C-ILK-RBPJ. I Confocal views of PrP^C and EGFR staining in H1975; white arrows mark overlap zones. Scale bar = 20 µm. J Heatmap of top differentially regulated genes in H1650 under PRNP siRNA ± recombinant EGF. qRT-PCR quantifying SNAI2 (k), ILK (l), JAG1, and RBPJ (m) transcripts in H1650 with PRNP siRNA ± EGF. N Immunoblot detecting RBPJ in H1650 under PRNP siRNA ± EGF. qRT-PCR and immunoblot data are means ± s.e.m from n = 2 independent triplicates. *p < 0.05, **p < 0.01, ***p < 0.001 vs. control (siScramble

or vehicle), # $p < 0.05$, ###$p < 0.001$ vs. TGFβ1- or EGF-exposed siScramble, §$p < 0.05$ vs. EGF-naïve knockdown. Immunoblot signals normalised to α-tubulin (α-tub).

After establishing a feed-forward interaction linking PrPC to EGFR signaling, we explored the potential influence of PrPC on EGFR function. Initial observations confirmed co-localization of PrPC and EGFR in H1975 cells **(Figure 5i),** aligning with prior documentation by Atkinson *et al*. in HT29 colorectal carcinoma cells [46]. We then assessed consequences of PRNP knockdown using siRNA in H1650 cells stimulated with EGF. Transcriptomic profiling via RNAseq demonstrated a profound disruption of the cellular reaction to EGF (25 ng/ml, 24 h) following PRNP suppression, as visualized in the heatmap **(Figure 5j).** Specifically, whereas EGF typically triggers an epithelial-mesenchymal transition (EMT) signature in H1650 cells, as documented elsewhere [37], PRNP depletion blunted this process, manifesting as diminished baseline expression and reduced upregulation of SNAI2 relative to untreated controls **(Figure 5k).** Additionally, cells lacking PrPC showed no induction of ILK or JAG1 upon EGF challenge, while RBPJ mRNA and protein were constitutively lower compared to controls **(Figures 5l-5n).** Taken together, these findings imply that PRNP transcription (i) is amplified through EGFR engagement, be it via oncogenic mutations or ligand stimulation, (ii) in turn amplifies EGFR signaling, and (iii) facilitates establishment and/or persistence of the mesenchymal phenotype.

PrPC correlates with acquired resistance to EGFR tyrosine kinase inhibitors in non-small cell lung cancer

Despite extensive evidence connecting PrPC to therapeutic refractoriness across multiple malignancies (summarized in [15]), its involvement in overcoming EGFR-directed agents in lung adenocarcinoma remained uncharted. This gap is noteworthy, given our demonstration that PrPC drives EMT, a well-recognized pathway mediating escape from EGFR blockade [47]. Re-analysis of data from Nilsson *et al*. [13] uncovered substantial upregulation of PRNP mRNA in three independent erlotinib-refractory HCC827 sublines versus the sensitive parent line **(Figure 6a).** Comparable elevation persisted in surviving fractions of HCC827 cells after dual osimertinib-trametinib exposure **(Figure 6b)** [25]. Parallel increases in PRNP transcripts emerged in HCC827 models of either short-term osimertinib challenge or chronic adaptation yielding persister states **(Figure 6c)** [26]. Intriguingly, ILK transcripts followed a similar pattern of enrichment in every resistant context examined. Functional validation in H1975 cells revealed that PRNP knockdown not only curtailed baseline proliferation **(Figure 2e**) but also markedly heightened vulnerability to osimertinib across dose levels **(Figure 6d).** Supporting clinical relevance, single-cell profiling from Maynard *et al*. indicated selective PRNP enrichment within malignant cells from EGFR-mutant cases displaying disease progression on EGFR inhibitors **(Figure 6e)** [28].

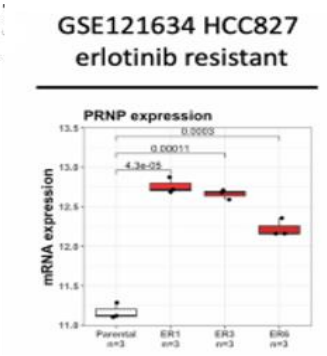

a)

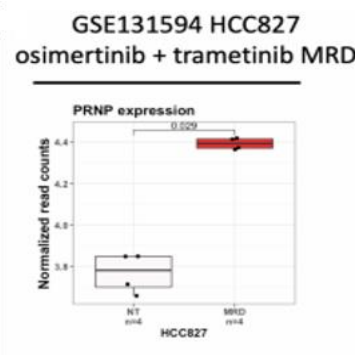

b)

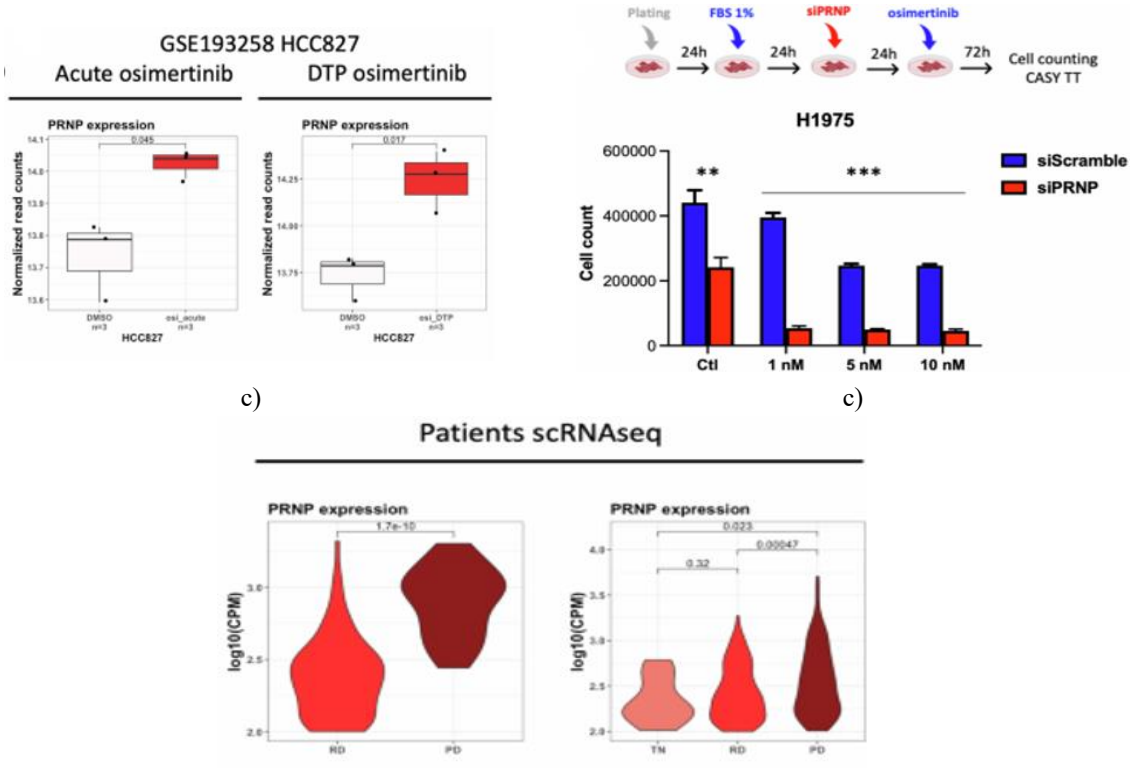

Figure 6. PRNP levels are associated with resistance to EGFR-TKI. Boxplots showing the distribution of PRNP mRNA in (a) erlotinib-resistant HCC827 clones versus parental cells (b) the minimal residual cell population obtained after combined treatment of HCC827 cells with osimertinib and trametinib (c) HCC827 cells acutely exposed to osimertinib (left) or HCC827 persister cells after long-term exposure osimertinib (right). d) Quantification of cell numbers in H1975 cells pre-treated or not with PRNP siRNA and exposed to different doses of osimertinib for 72 h, according to the schematic workflow (top). e) Differential expression of PRNP is shown in violin plots for single cancer cells collected from a patient treated with erlotinib (left) or a patient treated with osimertinib (right). TN treatment naive, RD residual disease, PD progressive disease.

Circulating PrPC concentrations are increased in EGFR-mutant non-small cell lung cancer and fluctuate in parallel with clinical course

We subsequently evaluated whether serial measurement of soluble PrPC might hold diagnostic or monitoring utility, building on precedents in colorectal malignancy [16]. Circulating PrPC was assayed in plasma from 29 individuals harboring EGFR-mutant advanced NSCLC commencing frontline tyrosine kinase inhibition. Pretreatment samples (T0) exhibited significantly greater PrPC abundance versus age- and gender-matched healthy volunteers **(Figures 7a and 7b).** A non-significant trend toward escalation was noted at metastatic progression (T0) among subsets with prior adjuvant chemotherapy for early-stage disease.

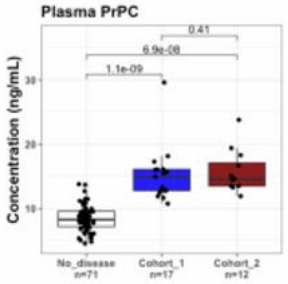

a)

Characteristic	Controls, N = 71[1]	Cohort 1, N = 17[1]	Cohort 2, N = 12[1]	p-value[2]
Plasma PrPC	8.3 (7.2, 9.6)	14.9 (12.8, 16.1)	14.6 (13.5, 17.1)	**<0.001**
Age	65 (55, 73)	65 (55, 75)	55 (52, 67)	0.3
Sex				0.9
F	45 (63%)	10 (59%)	8 (67%)	
M	26 (37%)	7 (41%)	4 (33%)	

[1]Median (IQR); n (%)

[2]Kruskal-Wallis rank sum test; Fisher's exact test

b)

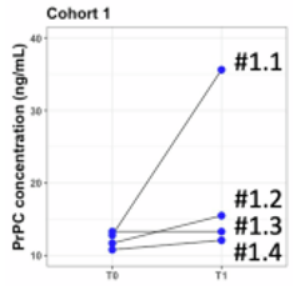

c)

Patient	Lesions at T0	Events at T1	Status at T1
# 1.1	Lung, Lymph nodes	Increase in pulmonary nodules (scanner)	Progression
# 1.2	Lung, Bones	Increase in bone lesions (scanner)	Progression
# 1.3	Lung, Lymph nodes, Liver	Progression: Increase in target lesions, non-target lesions and new lesions observed	Progression
# 1.4	Lung, Pleura	Increase in lung micronodules (scanner)	Progression

d)

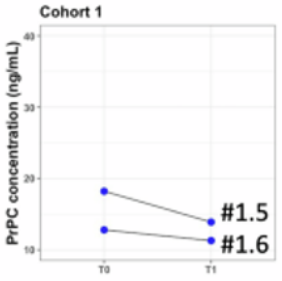

e)

Patient	Lesions at T0	Events at T1	Status at T1
# 1.5	Lung, Lymph nodes, Bones	Toxicity of chemotherapy – change of treatment – New secondary bone lesions (bone scan)	Toxicity
# 1.6	Lung, Lymph nodes, Bones, Brain	Stable peripheral disease - cerebral progression (MRI)	Stable

f)

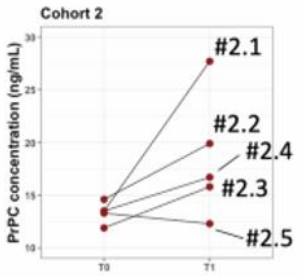

g)

Patient	Lesions at T0	Events at T1	Status at T1
# 2.1	Lung, Bone, Pleura, Lymph nodes, Brain	Bone progression in the sternum (scanner)	Progression
# 2.2	Lung, Lymph nodes, Brain, Adrenal	Brain progression (scanner)- del19 detected in LCR	Progression
# 2.3	Lung, Lymph nodes	RECIST progression of non-target lesions (scanner)	Progression
# 2.4	Lung, Pleura	Slow progression	Progression
# 2.5	Squamous CC, Lung, Bone, Liver, Adrenal	Squamous CC, Treatment evaluation, SD	Stable

h)

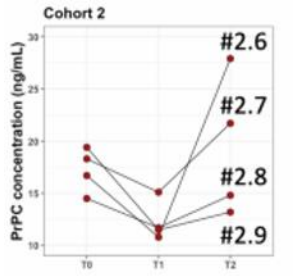

i)

Patient	Lesions at T0	Events at T1	Status at T1	Events at T2	Status at T2
# 2.6	Lung, Lymph nodes, Bone, Pleura, Adrenal, Muscle, Liver	Treatment first evaluation	Partial response	Bone Progression (scanner)	Progression
# 2.7	Lung, Lymph Nodes, Bones	Treatment first evaluation	Partial response	Stable disease	Stable
# 2.8	Lung, pleura	Treatment first evaluation	Partial response	Progression of non-target lesions (scanner)	Progression
# 2.9	Lung, Brain, Thorax	Treatment first evaluation	Partial response	RECIST Progression – Brain Progression	Progression

j)

Figure 7. Plasma PrPC levels are elevated in EGFR-mutant NSCLC patients and evolve according to disease history. a) Boxplot showing the mean levels of circulating PrPC in the plasma of healthy subjects or patients with EGFR-mutated NSCLC at the time of pre-treatment with first line EGFR-TKI in the metastatic disease. b) Summary of plasmatic PrPC values according to demographic information in healthy subjects or patients. c) Evolution of plasma PrPC levels in paired samples from EGFR-TKI treated patients from cohort 1 between pre-treatment (T0) and evaluation (T1) with T1 corresponding to progression. d) Table summarizing clinical data of patients from (c) at T0 and T1. E Evolution of plasma PrPC levels in paired samples from EGFR-TKI treated patients from cohort 1 between pre-treatment (T0) and evaluation (T1) with T1 corresponding to a clinical event other than progression. F Table summarizing clinical data of patients from (e) at T0 and T1. g)

Evolution of plasma PrPC levels in paired samples from EGFR-TKI patients from cohort 2 between pre-treatment (T0) and evaluation (T1). h) Table summarizing clinical data of patients from (g) at T0 and T1. I Kinetics of evolution of plasma PrPC levels in samples from EGFR-TKI patients from cohort 2 according to disease history. J Table summarizing clinical data of patients from (I) at T0, T1 and T2

Paired specimens were obtained from 6 PLAPOU patients at baseline (T0) and at the first progression (T1) during first-generation TKI therapy. Four individuals displayed stable (#1.3) or rising PrPC concentrations (#1.1, #1.2, and #1.4) **(Figure 7c),** concurrent with documented clinical progression **(Figure 7d).** A marked reduction in PrPC was observed from T0 to T1 in patient #1.5, who switched therapy due to intolerance, and a milder decline in patient #1.6, whose extracranial disease remained controlled **(Figures 7e and 7f).**

In the Onco-HEGP cohort, longitudinal data existed for 9 patients receiving frontline osimertinib. Five provided matched samples at pretreatment (T0) and initial progression (T1) **(Figure 7g).** PrPC concentrations rose in four cases and remained unchanged in one patient with verified stable disease **(Figures 7g and 7h).** The final cohort included trios of samples collected before first-line therapy (T0), at initial response assessment (T1), and at progression (T2). Strikingly, PrPC consistently declined at T1 and rebounded at T2 **(Figures 7i and 7j).** Additional details for patients #2.1 and #2.6 are presented as illustrative cases of disease tracking. Overall, these observations indicate that serial measurement of circulating PrPC during treatment may offer objective insight into disease trajectory.

The cellular and molecular bases underlying acquired resistance to tyrosine kinase inhibitors in EGFR-mutant lung adenocarcinoma are incompletely defined. Epithelial-mesenchymal transition (EMT) stands out among non-mutational mechanisms [3], prompting inquiry into its triggers. This study evaluated PrPC as a driver of EMT in EGFR-mutant lung adenocarcinoma. PrPC, a glycosylphosphatidylinositol-anchored protein long investigated for its role in prion disorders [48], is increasingly recognised in oncology for promoting migration, invasion, and resistance to chemotherapy and radiotherapy [15].

Evidence that PrPC drives EMT derives from integrated bioinformatic and functional analyses. Interrogation of the CCLE repository alongside four clinical datasets, including the Onco-HEGP series, repeatedly revealed robust associations between PRNP expression and mesenchymal signatures. Functional experiments established that PrPC is required for both induction (via TGFβ or EGF stimulation) and sustenance of mesenchymal characteristics. Mechanistically, rather than modulating secreted TGFβ abundance—as previously observed in colorectal carcinoma [16]—PrPC sensitises NSCLC cells to TGFβ signalling. Through orchestration of an ILK-RBPJ module, PrPC establishes a receptive cellular state enabling robust induction of EMT transcription factors like ZEB1 upon TGFβ exposure. These findings align with (i) prior identification of ILK as a direct PrPC effector [18], (ii) detection of ILK among PrPC interactors in melanoma, (iii) tight co-expression of PrPC and ILK in lung and colon adenocarcinoma (unpublished data), and (iv) adverse prognostic impact of elevated ILK in EGFR-mutant NSCLC [49]. Concerning RBPJ, the results echo PrPC-mediated modulation of Notch signalling during neural differentiation [34] and in pancreatic malignancy [35]. Consistency across NSCLC models and the PC3 prostate line reinforces the conclusions. Given reports that ZEB1 upregulates NOTCH1 [50] and JAG1 [51] via miR-200 repression, PrPC, ZEB1, and Notch components likely form an interconnected regulatory circuit promoting EMT. This framework accommodates the elevated PRNP observed in Onco-HEGP cases exhibiting depressed miR-200 activity.

Another key insight is bidirectional crosstalk between PrPC and EGFR. We demonstrated that EGFR activation transcriptionally induces PRNP, accounting for its enrichment in EGFR-mutant tumours. This mechanism partially explains PrPC upregulation in lung adenocarcinoma, though additional pathways may contribute. Potential amplifiers include autoregulatory circuits involving TGFβ [16], ILK [18], Notch [34], Wnt, or glucocorticoid pathways [52].

Such self-reinforcement could explain sustained PRNP elevation after prolonged—but not acute—TGFβ stimulation. Conversely, PrPC exerts positive control over EGFR abundance and activity, recapitulating effects documented in neuroblastoma [53] and neural/dental stem cells [35, 54, 55]. Co-localisation of PrPC and EGFR in lung adenocarcinoma cells **(Figure 5i)** and diverse other contexts [46, 53] suggests PrPC influences EGFR trafficking or signal duration, as proposed earlier [56]. Dedicated studies are warranted to dissect this relationship further.

Lastly, we provide compelling evidence tying PrPC to EGFR-TKI refractoriness. Support includes (i) PRNP upregulation across multiple in vitro resistance models **(Figures 6a-6c),** (ii) enhanced osimertinib cytotoxicity

upon PrPC depletion in H1975 cells **(Figure 6d),** and (iii) selective PRNP enrichment in tumour cells from progressing versus residual disease states in treated patients **(Figure 6e).** Critically, serial plasma PrPC quantification in two independent cohorts demonstrated baseline elevation versus healthy controls and dynamic changes anticipating clinical progression. Analogous to our prior colorectal findings [16], rising circulating PrPC heralded worsening disease, irrespective of cellular origin.

Conclusion

In summary, this investigation positions PrPC as a critical node connecting EMT induction and EGFR-TKI escape in lung adenocarcinoma, while proposing plasma PrPC tracking as a minimally invasive monitoring tool. Coupled with earlier evidence that PrPC blockade impairs tumour growth [57], these results nominate PrPC as an attractive therapeutic candidate in EGFR-mutant disease.

Acknowledgments: None

Conflict of Interest: None

Financial Support: None

Ethics Statement: None

References

1. Sung H, Ferlay J, Siegel RL, Laversanne M, Soerjomataram I, Jemal A, et al. Global Cancer Statistics 2020: GLOBOCAN estimates of incidence and mortality worldwide for 36 cancers in 185 countries. CA Cancer J Clin. 2021;71:209–49. doi: 10.3322/caac.21660
2. Yang C-Y, Yang JC-H, Yang P-C. Precision management of advanced non-small cell lung cancer. Annu Rev Med. 2020;71:117–36. doi: 10.1146/annurev-med-041519-044330
3. Rotow J, Bivona TG. Understanding and targeting resistance mechanisms in NSCLC. Nat Rev Cancer. 2017;17:637–58. doi: 10.1038/nrc.2017.51
4. Passaro A, Jänne PA, Mok T, Peters S. Overcoming therapy resistance in EGFR-mutant lung cancer. Nat Cancer. 2021;2:377–91. doi: 10.1038/s41925-021-00374-7
5. Sequist LV, Waltman BA, Dias-Santagata D, Digumarthy S, Turke AB, Fidias P, et al. Genotypic and histological evolution of lung cancers acquiring resistance to EGFR inhibitors. Sci Transl Med. 2011;3:75ra26. doi: 10.1126/scitranslmed.3001003
6. Zhang Z, Lee JC, Lin L, Olivas V, Au V, LaFramboise T, et al. Activation of the AXL kinase causes resistance to EGFR-targeted therapy in lung cancer. Nat Genet. 2012;44:852–60. doi: 10.1038/ng.2350
7. Weng C-H, Chen L-Y, Lin Y-C, Shih J-Y, Lin Y-C, Tseng R-Y, et al. Epithelial-mesenchymal transition (EMT) beyond EGFR mutations per se is a common mechanism for acquired resistance to EGFR TKI. Oncogene. 2019;38:455–68. doi: 10.1038/s41388-018-0313-6
8. Aissa AF, Islam ABMMK, Ariss MM, Go CC, Rader AE, Conrardy RD, et al. Single-cell transcriptional changes associated with drug tolerance and response to combination therapies in cancer. Nat Commun. 2021;12:1628. doi: 10.1038/s41467-021-21957-4
9. Bronte G, Bravaccini S, Bronte E, Burgio MA, Rolfo C, Delmonte A, et al. Epithelial-to-mesenchymal transition in the context of epidermal growth factor receptor inhibition in non-small-cell lung cancer. Biol Rev Camb Philos Soc. 2018;93:1735–46. doi: 10.1111/brv.12411
10. Zhu X, Chen L, Liu L, Niu X. EMT-mediated acquired EGFR-TKI resistance in NSCLC: mechanisms and strategies. Front Oncol. 2019;9:1044. doi: 10.3389/fonc.2019.01044
11. Raoof S, Mulford IJ, Frisco-Cabanos H, Nangia V, Timonina D, Labrot E, et al. Targeting FGFR overcomes EMT-mediated resistance in EGFR mutant non-small cell lung cancer. Oncogene. 2019;38:6399–413. doi: 10.1038/s41388-019-0809-7
12. Yochum ZA, Cades J, Wang H, Chatterjee S, Simons BW, O'Brien JP, et al. Targeting the EMT transcription factor TWIST1 overcomes resistance to EGFR inhibitors in EGFR-mutant non-small-cell lung cancer. Oncogene. 2019;38:656–70. doi: 10.1038/s41388-018-0297-1

13. Nilsson MB, Sun H, Robichaux J, Pfeifer M, McDermott U, Travers J, et al. A YAP/FOXM1 axis mediates EMT-associated EGFR inhibitor resistance and increased expression of spindle assembly checkpoint components. Sci Transl Med. 2020;12:eaaz4589. doi: 10.1126/scitranslmed.aaz4589
14. Tulchinsky E, Demidov O, Kriajevska M, Barlev NA, Imyanitov E. EMT: A mechanism for escape from EGFR-targeted therapy in lung cancer. Biochim Biophys Acta Rev Cancer. 2019;1871:29–39. doi: 10.1016/j.bbcan.2018.11.006
15. Mouillet-Richard S, Ghazi A, Laurent-Puig P. The cellular prion protein and the hallmarks of cancer. Cancers. 2021;13:5032. doi: 10.3390/cancers13205032
16. Le Corre D, Ghazi A, Balogoun R, Pilati C, Aparicio T, Martin-Lannerée S, et al. The cellular prion protein controls the mesenchymal-like molecular subtype and predicts disease outcome in colorectal cancer. EBioMedicine. 2019;46:94–104. doi: 10.1016/j.ebiom.2019.08.035
17. Lin S-C, Lin C-H, Shih N-C, Liu H-L, Wang W-C, Lin K-Y, et al. Cellular prion protein transcriptionally regulated by NFIL3 enhances lung cancer cell lamellipodium formation and migration through JNK signaling. Oncogene. 2020;39:385–98. doi: 10.1038/s41388-019-0994-6
18. Ghazi A, Le Corre D, Pilati C, Taieb J, Aparicio T, Didelot A, et al. Prognostic value of the PrPC-ILK-IDO1 axis in the mesenchymal colorectal cancer subtype. Oncoimmunology. 2021;10:1940674. doi: 10.1080/2162402X.2021.1940674
19. Dobin A, Davis CA, Schlesinger F, Drenkow J, Zaleski C, Jha S, et al. STAR: ultrafast universal RNA-seq aligner. Bioinformatics. 2013;29:15–21. doi: 10.1093/bioinformatics/bts635
20. Barretina J, Caponigro G, Stransky N, Venkatesan K, Margolin AA, Kim S, et al. The Cancer Cell Line Encyclopedia enables predictive modelling of anticancer drug sensitivity. Nature. 2012;483:603–7. doi: 10.1038/nature10866
21. Cancer Genome Atlas Research Network. Comprehensive molecular profiling of lung adenocarcinoma. Nature. 2014;511:543–50. doi: 10.1038/nature13385
22. Garinet S, Didelot A, Denize T, Perrier A, Beinse G, Leclere J-B, et al. Clinical assessment of the miR-34, miR-200, ZEB1 and SNAIL EMT regulation hub underlines the differential prognostic value of EMT miRs to drive mesenchymal transition and prognosis in resected NSCLC. Br J Cancer. 2021;125:1544–51. doi: 10.1038/s41416-021-01503-7
23. Lehtiö J, Arslan T, Siavelis I, Pan Y, Socciarelli F, Berkovska O, et al. Proteogenomics of non-small cell lung cancer reveals molecular subtypes associated with specific therapeutic targets and immune evasion mechanisms. Nat Cancer. 2021;2:1224–42. doi: 10.1038/s41925-021-00486-x
24. Garinet S, Didelot A, Marisa L, Beinse G, Sroussi M, Le Pimpec-Barthes F, et al. A novel Chr1-miR-200 driven whole transcriptome signature shapes tumor immune microenvironment and predicts relapse in early-stage lung adenocarcinoma. J Transl Med. 2023;21:324. doi: 10.1186/s12967-023-04139-4
25. Kurppa KJ, Liu Y, To C, Zhang T, Fan M, Vajdi A, et al. Treatment-induced tumor dormancy through YAP-mediated transcriptional reprogramming of the apoptotic pathway. Cancer Cell. 2020;37:104–22.e12. doi: 10.1016/j.ccell.2019.11.008
26. Gogleva A, Polychronopoulos D, Pfeifer M, Poroshin V, Ughetto M, Martin MJ, et al. Knowledge graph-based recommendation framework identifies drivers of resistance in EGFR mutant non-small cell lung cancer. Nat Commun. 2022;13:1667. doi: 10.1038/s41467-022-29396-w
27. Regales L, Gong Y, Shen R, de Stanchina E, Vivanco I, Goel A, et al. Dual targeting of EGFR can overcome a major drug resistance mutation in mouse models of EGFR mutant lung cancer. J Clin Investig. 2009;119:3000–10. doi: 10.1172/JCI38536
28. Maynard A, McCoach CE, Rotow JK, Harris L, Haderk F, Kerr DL, et al. Therapy-induced evolution of human lung cancer revealed by single-cell RNA sequencing. Cell. 2020;182:1232–51.e22. doi: 10.1016/j.cell.2020.07.011
29. Pécuchet N, Zonta E, Didelot A, Combe P, Thibault C, Gibault L, et al. Base-position error rate analysis of next-generation sequencing applied to circulating tumor DNA in non-small cell lung cancer: a prospective study. PLoS Med. 2016;13:e1002199. doi: 10.1371/journal.pmed.1002199
30. Chen Y-J, Roumeliotis TI, Chang Y-H, Chen C-T, Han C-L, Lin M-H, et al. Proteogenomics of non-smoking lung cancer in East Asia delineates molecular signatures of pathogenesis and progression. Cell. 2020;182:226–44.e17. doi: 10.1016/j.cell.2020.06.029

31. Mak MP, Tong P, Diao L, Cardnell RJ, Gibbons DL, William WN, et al. A patient-derived, pan-cancer EMT signature identifies global molecular alterations and immune target enrichment following epithelial-to-mesenchymal transition. Clin Cancer Res J Am Assoc Cancer Res. 2016;22:609–20. doi: 10.1158/1078-0432.CCR-15-1064
32. de Reyniès A, Jaurand M-C, Renier A, Couchy G, Hysi I, Elarouci N, et al. Molecular classification of malignant pleural mesothelioma: identification of a poor prognosis subgroup linked to the epithelial-to-mesenchymal transition. Clin Cancer Res. 2014;20:1323–34. doi: 10.1158/1078-0432.CCR-13-1607
33. Sun Y, Daemen A, Hatzivassiliou G, Arnott D, Wilson C, Zhuang G, et al. Metabolic and transcriptional profiling reveals pyruvate dehydrogenase kinase 4 as a mediator of epithelial-mesenchymal transition and drug resistance in tumor cells. Cancer Metab. 2014;2:20. doi: 10.1186/2049-3002-2-20
34. Martin-Lannerée S, Halliez S, Hirsch TZ, Hernandez-Rapp J, Passet B, Tomkiewicz C, et al. The cellular prion protein controls notch signaling in neural stem/progenitor cells. Stem Cells. 2017;35:754–65. doi: 10.1002/stem.2592
35. Wang Y, Yu S, Huang D, Cui M, Hu H, Zhang L, et al. Cellular prion protein mediates pancreatic cancer cell survival and invasion through association with and enhanced signaling of Notch1. Am J Pathol. 2016;186:2945–56. doi: 10.1016/j.ajpath.2016.06.007
36. Derynck R, Muthusamy BP, Saeteurn KY. Signaling pathway cooperation in TGF-β-induced epithelial-mesenchymal transition. Curr Opin Cell Biol. 2014;31:56–66. doi: 10.1016/j.ceb.2014.02.005
37. Hori K, Sen A, Artavanis-Tsakonas S. Notch signaling at a glance. J Cell Sci. 2013;126:2135–40. doi: 10.1242/jcs.096268
38. Sethi N, Dai X, Winter CG, Kang Y. Tumor-derived JAGGED1 promotes osteolytic bone metastasis of breast cancer by engaging notch signaling in bone cells. Cancer Cell. 2011;19:192–205. doi: 10.1016/j.ccr.2011.01.004
39. Manderfield LJ, High FA, Engleka KA, Liu F, Li L, Rentschler S, et al. Notch activation of Jagged1 contributes to the assembly of the arterial wall. Circulation. 2012;125:314–23. doi: 10.1161/CIRCULATIONAHA.111.044666
40. Li H, Zhang J, Ke J-R, Yu Z, Shi R, Gao S-S, et al. Pro-prion, as a membrane adaptor protein for E3 ligase c-Cbl, facilitates the ubiquitination of IGF-1R, promoting melanoma metastasis. Cell Rep. 2022;41:111834. doi: 10.1016/j.celrep.2022.111834
41. Troussard AA, McDonald PC, Wederell ED, Mawji NM, Filipenko NR, Gelmon KA, et al. Preferential dependence of breast cancer cells versus normal cells on integrin-linked kinase for protein kinase B/Akt activation and cell survival. Cancer Res. 2006;66:393–403. doi: 10.1158/0008-5472.CAN-05-2832
42. Jiang H, Zhou C, Zhang Z, Wang Q, Wei H, Shi W, et al. Jagged1-Notch1-deployed tumor perivascular niche promotes breast cancer stem cell phenotype through Zeb1. Nat Commun. 2020;11:5129. doi: 10.1038/s41467-020-18932-0
43. Maciaczyk D, Picard D, Zhao L, Koch K, Herrera-Rios D, Li G, et al. CBF1 is clinically prognostic and serves as a target to block cellular invasion and chemoresistance of EMT-like glioblastoma cells. Br J Cancer. 2017;117:102–12. doi: 10.1038/bjc.2017.125
44. Pallier K, Cessot A, Côté J-F, Just P-A, Cazes A, Fabre E, et al. TWIST1 a new determinant of epithelial to mesenchymal transition in EGFR mutated lung adenocarcinoma. PLoS ONE. 2012;7:e29954. doi: 10.1371/journal.pone.0029954
45. Andreu-Agullo C, Morante-Redolat JM, Delgado AC, Farinas I. Vascular niche factor PEDF modulates Notch-dependent stemness in the adult subependymal zone. Nat Neurosci. 2009;12:1514–23. doi: 10.1038/nn.2433
46. Atkinson CJ, Kawamata F, Liu C, Ham S, Győrffy B, Munn AL, et al. EGFR and Prion protein promote signaling via FOXO3a-KLF5 resulting in clinical resistance to platinum agents in colorectal cancer. Mol Oncol. 2019;13:725–37. doi: 10.1002/1878-0261.12444
47. Zhang X, Maity TK, Ross KE, Qi Y, Cultraro CM, Bahta M, et al. Alterations in the global proteome and phosphoproteome in third generation EGFR TKI resistance reveal drug targets to circumvent resistance. Cancer Res. 2021;81:3051–66. doi: 10.1158/0008-5472.CAN-20-1589
48. Aguzzi A, Baumann F, Bremer J. The prion's elusive reason for being. Annu Rev Neurosci. 2008;31:439–77. doi: 10.1146/annurev.neuro.31.102607.144115

49. Karachaliou N, Cardona AF, Bracht JWP, Aldeguer E, Drozdowskyj A, Fernandez-Bruno M, et al. Integrin-linked kinase (ILK) and src homology 2 domain-containing phosphatase 2 (SHP2): novel targets in EGFR-mutation positive non-small cell lung cancer (NSCLC). EBioMedicine. 2019;39:207–14. doi: 10.1016/j.ebiom.2019.01.040
50. Zhang T, Guo L, Creighton CJ, Lu Q, Gibbons DL, Yi ES, et al. A genetic cell context-dependent role for ZEB1 in lung cancer. Nat Commun. 2016;7:12231. doi: 10.1038/ncomms12231
51. Brabletz S, Bajdak K, Meidhof S, Burk U, Niedermann G, Firat E, et al. The ZEB1/miR-200 feedback loop controls Notch signalling in cancer cells. EMBO J. 2011;30:770–82. doi: 10.1038/emboj.2011.3
52. Mouillet-Richard S, Gougelet A, Passet B, Brochard C, Le Corre D, Pitasi CL, et al. Wnt, glucocorticoid and cellular prion protein cooperate to drive a mesenchymal phenotype with poor prognosis in colon cancer. J Transl Med. 2024;22:337. doi: 10.1186/s12967-024-05022-2
53. Llorens F, Carulla P, Villa A, Torres JM, Fortes P, Ferrer I, et al. PrP© regulates epidermal growth factor receptor function and cell shape dynamics in Neuro2a cells. J Neurochem. 2013;127:124–38. doi: 10.1111/jnc.12380
54. Martellucci S, Manganelli V, Santacroce C, Santilli F, Piccoli L, Sorice M, et al. Role of Prion protein-EGFR multimolecular complex during neuronal differentiation of human dental pulp-derived stem cells. Prion. 2018;12:117–26. doi: 10.1080/19335089.2018.1467541
55. Groveman BR, Schwarz B, Bohrnsen E, Foliaki ST, Carroll JA, Wood AR, et al. A PrP EGFR signaling axis controls neural stem cell senescence through modulating cellular energy pathways. J Biol Chem. 2023;299:105319. doi: 10.1016/j.jbc.2023.105319
56. Solis GP, Schrock Y, Hulsbusch N, Wiechers M, Plattner H, Stuermer CA. Reggies/flotillins regulate E-cadherin-mediated cell contact formation by affecting EGFR trafficking. Mol Biol Cell. 2012;23:1812–25. doi: 10.1091/mbc.E111-10-0877
57. Mouillet-Richard S, Martin-Lannerée S, Le Corre D, Hirsch TZ, Ghazi A, Sroussi M, et al. A proof of concept for targeting the PrPC - Amyloid βpeptide interaction in basal prostate cancer and mesenchymal colon cancer. Oncogene. 2022;41:4397–404. doi: 10.1038/s41388-022-02366-3